A Laboratory Study of the Effect of Acetic Acid Vapor on Atmospheric Copper Corrosion

A. López-Delgado, E. Cano, J. M. Bastidas,* and F. A. López

Centro Nacional de Investigaciones Metalúrgicas, 28040 Madrid, Spain

ABSTRACT

A study was made of the copper corrosion rate and corrosion products originated by the action of acetic acid vapor at 100% relative humidity. Copper plates were exposed to an acetic acid contaminated atmosphere for a period of 21 days. Five acetic vapor concentration levels were used. The copper corrosion rate was in the range of 1 to 23 mg/dm^2 day. The corrosion-product layers were characterized using electrochemical, X-ray powder diffraction, Fourier transform infrared spectrometry, and scanning electron microscopy techniques. Thermal and calorimetric studies were also performed. Some of the compounds identified were cuprite (Cu_2O), copper acetate hydrate [$Cu(CH_3COO)_2 \cdot 2H_2O$], and copper hydroxide acetate [$Cu_4(OH)(CH_3COO)_7 \cdot 2H_2O$]. This last compound was also characterized. The thickness of the patina layers was 4 to 8 nm for amorphous cuprite, 11 to 48 nm for cuprite, and 225 nm for copper acetate. The patina, in which the cementation process of different corrosion-product layers plays an important role, is formed by the reaction of acetic vapor with copper through porous cuprite paths.

Introduction

The corrosion originated by organic acid vapors on different metals and alloys is a phenomenon which has been observed for a long time. The influence of organic acid vapors on copper structures after prolonged exposure in a town atmosphere was studied by Vernon.[1] The presence of these acids in the outdoor atmosphere is a source of free acidity in precipitation in industrial areas.[2-6] Acetic acid is emitted by the industries themselves.[7] Acetic vapor is also present in industrial atmospheres, e.g., from vinegar in the food processing industry and from the decomposition of raw materials in the paper industry. Organic acid anions constitute about 0.1 to 1% of the total ion concentration in the corrosion-products (patina) on copper exposed to the outdoor atmosphere for extended periods.[8] In the case of packaged metal, acetic acid vapor is released by woods and certain paints, plastics, rubbers, resins, and other materials likely to be found alongside packaged metal items.[7,9-15] An important aspect of acetic acid vapor is that it causes metal corrosion at very low concentrations.[16-19]

The aim of this paper is to study the corrosion behavior of copper exposed for short periods of time to acetic acid vapor in laboratory experiments at 100% relative humidity. The solid phases formed on copper surfaces were analyzed in order to elucidate the influence of acetic acid vapor on the patination process mechanism.

Experimental

Generation of acetic vapor.—Corrosive environments were generated in an airtight 2.4 L glass vessel. In order to obtain a vapor concentration of acetic acid, it was assumed that the partial pressure of solvent vapor in equilibrium with a dilute solution is directly proportional to the mole fraction of solvent in the solution

$$P = \chi P_0 \qquad [1]$$

which is the expression of Raoult's law,[20] where P is the partial pressure of the solvent (acetic acid in this case) above the solution (in Pa), P_0 is the vapor pressure of the pure solvent (acetic acid in this case), and χ is the mole fraction of solvent in the aqueous solution (pure acetic acid and distilled water).

The concentration of acetic acid in the vapor phase (C), expressed in parts per million (ppm), (10^6, by weight), can be written as

$$C = \frac{\left(\frac{P}{101{,}300}\right)60}{29} 10^6 = 20.4P \qquad [2]$$

where 60 is the molecular weight of acetic acid, the 101,300 term is the amount of Pa in one atmosphere, and 29 is the molecular weight of air.

If G is the mass of acetic acid, expressed as number of grams in a 1000 mL solution, then χ can be written as

$$\chi \approx \frac{G/60}{1000/18} = 3 \times 10^{-4} G \qquad [3]$$

where 18 is the molecular weight of water.

Taking into account Eq. 1, 2, and 3, it is possible to write

$$\frac{C}{20.4} = 3 \times 10^{-4} G P_0 \qquad [4]$$

therefore

$$G = 163.2 \frac{C}{P_0} \qquad [5]$$

The P_0 value was obtained from Fig. 1. This was drawn using data from the literature[21] and the Claussius-Clapeyron equation ($\log P_0 = -A/T + B$).[22]

The relative humidity (RH) of approximately 100% was obtained by placing 350 mL of distilled water in the bottom of the airtight glass vessel, with the copper specimens placed on a perforated ceramic grill situated above the distilled water.

Five acetic acid concentrations: 10, 50, 100, 200, and 300 ppm were studied. The vapor concentration of acetic acid was obtained by replacing the 350 mL of distilled water at the bottom of the airtight glass vessel with a solution containing the appropriate amount of glacial acetic acid (Merck): G in Eq. 5. These levels were chosen in order to accelerate the corrosion process in the laboratory with the aim of following the evolution process of the patina from its origin stage up to 21 days experimentation.

In order to obtain experimental conditions with high reproducibility, i.e., a constant concentration of acetic vapor

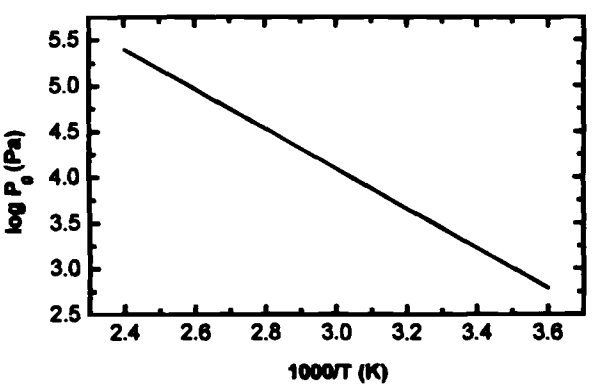

Fig. 1. Acetic acid vapor pressure against temperature.

* Electrochemical Society Active Member.

during the experiments, the acetic aqueous solution was changed once a week.

Specimens.—The copper used had the following chemical composition (wt %): 0.015 Pb, 0.009 Sn, <0.001 Al, <0.002 Sb, <0.001 As, <0.001 Bi, <0.001 Fe, 0.003 Ni, 0.019 P, <0.001 Mn, balance Cu. The copper was phosphorus-deoxidized with low residual phosphorus content (Type Cu-DLP, Standard ISO 1337).

Mechanically polished specimens were prepared with different grades of emery paper down to grade 600. The experimental details have been described elsewhere.[22]

Vertically suspended 5 × 5 cm copper plates were exposed to the action of acetic acid vapor for a period of 21 days. The temperature was maintained at 30°C during the experiments by immersing the airtight glass vessel in a thermostatically controlled water bath. At the end of these experiments the nature of the surface corrosion products was determined. For comparative purposes, a copper reference specimen was exposed to an uncontaminated 100% RH atmosphere under identical experimental conditions.

Techniques.—Gravimetric analyses were carried out taking measurements at the beginning of the experiments and at their end, following the removal of the corrosion products using a 10% H_2SO_4 aqueous solution, in accordance with ASTM Standard G1-88. All the experiments were performed in triplicate, i.e., the gravimetric corrosion rate is listed as an average value of three specimens studied under identical experimental conditions. The reproducibility of the experimental gravimetric results was higher than 90%. An electronic analytical balance with a precision of ±0.1 mg was used.

Electrochemical studies were performed by cathodic reduction using a EG&G PARC, model 273A potentiostat/galvanostat. The classic three-electrode configuration was used, employing a saturated calomel electrode (SCE) as reference and a spiral AISI 316L stainless steel wire as the counter electrode. The surface of the specimen was masked using a corrosion protection tape, leaving an uncovered area of 1 cm^2 as the working electrode. Experiments were carried out under static conditions at room temperature. A 0.1 M sodium borate solution, 500 mL, pH close to 9 and analytical grade, was used as supporting electrolyte for the cathodic reduction experiments.[23-25] The solution was deaerated by bubbling nitrogen through the system for 1 h before the start of experimentation and throughout its duration.

The solid phases formed on the copper surface were characterized by X-ray powder diffraction (XRD), employing a Siemens D-500 diffractometer with monochromatized Cu Kα radiation. Patterns were recorded in the step scanning mode, with a 0.025° (2θ) step and 2 s counting time.

A Nicolet Magna 550 (CsI beam splitter) spectrophotometer was used to record Fourier transform infrared (FTIR) spectra on CsI disks. The wavenumber range was 4000-270 cm^{-1}.

A JEOL JXA-840 scanning electron microscope (SEM) was used to perform morphological observations. Conducting samples for SEM were prepared by gold sputtering the copper plates.

A thermodifferential analyzer (DTA) and a thermogravimetric analyzer (TG), Shimazdu DTA-50 and TGA-50H, respectively, were employed to determine the thermal behavior and the evolution of the solids formed on the surface layer as a function of temperature. Tests were carried out in a dynamic air atmosphere (20 mL/min) at a heating rate of 10°C/min. Alumina crucibles were used in both types of analysis. These thermal studies were performed only on specimens from experiments with an atmospheric acetic level of more than 100 ppm which provided an adequate amount of solid corrosion products.

Results and Discussion

The visual appearance of the copper specimens exposed to the action of acetic acid vapors alters as the contamination level increases. Thus, a new freshly cleaned copper surface of bright salmon-pink color, after exposure to an uncontaminated 100% RH atmosphere, maintains its color though its brightness disappears. After exposure to a 10 ppm acetic vapor atmosphere, the copper surface shows a dull brown shade, indicating that copper patina is starting to form. On copper specimens exposed to the 50 ppm acetic vapor atmosphere, a brownish-gray layer is observed. A large number of very small nonuniform size spots are deposited on this layer. Some of these are dark green in color, and the others are of a dark grayish-brown color. The copper specimens exposed to the 100 ppm acetic vapor atmosphere exhibit solids of a pale green and dark green color deposited on the brownish-gray layer. On copper specimens exposed to the 200 ppm acetic vapor atmosphere, a dark green solid is observed to be deposited on the first brownish-gray layer. The amount of solids formed is greater than with the previous specimen. At the highest acetic contamination level studied, 300 ppm, a uniform greenish-blue velvet-like layer was formed. The formation of this last color layer may be associated with an advanced step of the patination process.[26]

Electrochemical and gravimetric analyses.—Figure 2 reports the corrosion rate estimated from gravimetric data, expressed as mg/dm^2/day (mdd), for copper exposed to acetic acid vapor for 21 days experimentation time, with a corrosion rate of up to 23 mdd. It can be observed that the copper corrosion rate increases in line with the increase in acetic concentration. There seems to be an acetic vapor contamination threshold, 200 ppm, above which the corrosion rate stabilizes. The rate stabilization may be related to the formation of a copper compound which protects the copper surface, probably a copper acetate compound (as shown by XRD later in the text). In all exposure conditions, during the first week of experimentation, the blue crystals were surrounded by zones free of corrosion products which could act as cathodic areas.[22] After 21 days exposure, all the copper surface was covered with corrosion products. Visually the specimens appeared to be covered with a layer of nonadherent solid corrosion products of porous nature.

Cathodic reduction curves for copper samples exposed to 10, 100, and 300 ppm acetic vapor are depicted in Fig. 3, 4, and 5, respectively, for several exposure times. In Fig. 3, three peaks can be observed in the plot corresponding to 1 day of exposure. A first peak, located at −0.6 V_{SCE}, has been attributed to the reduction of amorphous cuprous oxide (cuprite, Cu_2O).[27-30] This Cu_2O layer is frequently formed by copper exposure to uncontaminated air. A second peak can be observed at −0.71 V_{SCE} which is attrib-

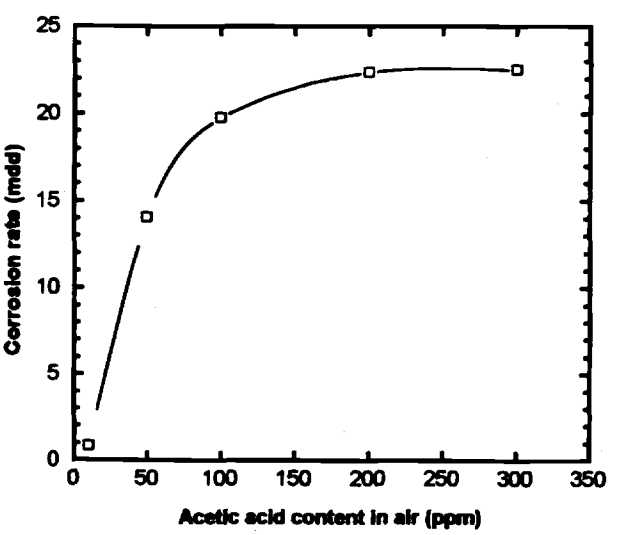

Fig. 2. Copper corrosion rate against acetic acid content in the atmosphere of an airtight 2.4 L glass vessel, after 21 days' exposure at 100% relative humidity and 30°C temperature.

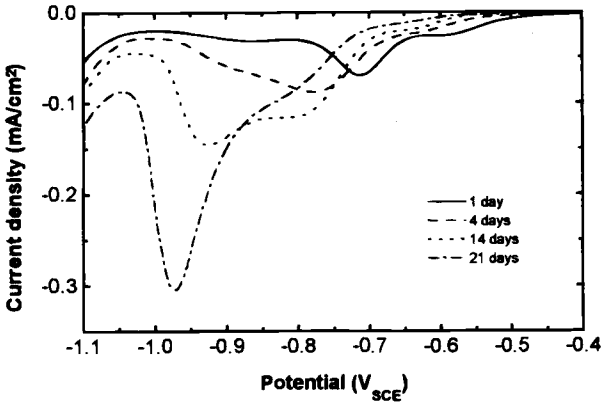

Fig. 3. Reduction scans in a 0.1 M deaerated sodium borate solution for copper exposed to 10 ppm acetic acid vapor. The scans were obtained at a potential sweep rate of 1 mV/s starting at the open-circuit potential.

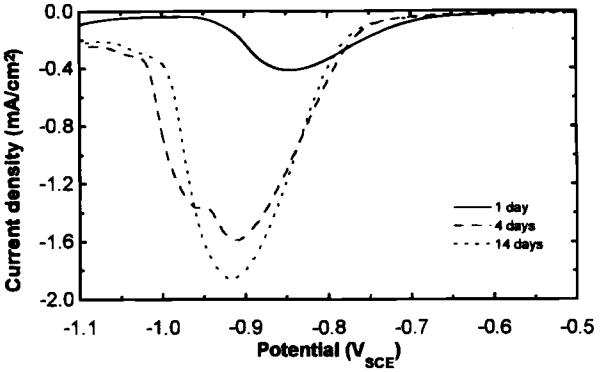

Fig. 5. Reduction scans in a 0.1 M deaerated sodium borate solution for copper exposed to 300 ppm acetic acid vapor. The scans were obtained at a potential sweep rate of 1 mV/s starting at the open-circuit potential.

uted to the reduction of crystalline cuprite formed on the initial amorphous cuprite.[29-33] The existence of these two cuprite peaks is corroborated by SEM observations (see below) and has been previously reported in the literature.[29,30] Finally, a third peak can be observed at approximately -0.9 V_{SCE}, which should be attributed to copper acetate, as is explained later in the text. Similar information was obtained for 4, 14, and 21 days experimentation time (see Fig. 3).

The area under the peak at -0.6 V_{SCE}, corresponding to amorphous Cu_2O (Fig. 3), decreases as the experimental time increases, and thus it may be interpreted that the thickness of the amorphous cuprite layer decreases throughout the 21 days tested. On the other hand, this peak evolution could be within the margin of error of the measurements. It should be said that as the time increases the peak corresponding to copper acetate is better defined and the area under the peak increases.

Figures 4 and 5 show, in general, similar information to Fig. 3. The copper acetate peak masks the other reduction peaks as the concentration of acetic vapor increases. A shoulder can be observed at -0.95 V_{SCE} in the plots for 4 days of exposure (Fig. 5) and for 14 days experimentation (Fig. 4), which may be ascribed to copper hydroxide acetate (see below).

In Fig. 3 the peaks at -0.7 and -0.9 V_{SCE} show growth at a comparable rate up to 14 days, but for 21 days the peak at -0.9 V_{SCE} indicates faster growth. In Fig. 4 after 4 days, it looks like the crystalline cuprite phase has grown but the copper acetate phase has not changed. By 14 days, significant growth has occurred in both the crystalline cuprite and copper acetate phases. By day 21, one peak is dominating. In Fig. 5 after 4 days, significant growth has occurred in the copper acetate phase. These results (Fig. 3 to 5) may be interpreted as different patination mechanisms as the acetic vapor concentration increases (see below).

In general, Fig. 3 to 5 show a potential peak shift to more cathodic values with time and acetic vapor content in the air increasing. This behavior may probably be associated with the thickening of the corrosion-products layer. It can also be observed that the copper acetate peak area increases without there being a decrease in the cuprite peak area. This is experimental evidence that the formation of copper acetate is not at the expense of the cuprite layer. The copper acetate is probably formed by the reaction of acetic acid vapor with copper through porous cuprite paths.

Figure 6 shows the recorded potential against time curve for the cathodic stripping of copper exposed to 10 ppm of acetic acid vapor using a 0.1 M deaerated sodium borate solution as supporting electrolyte. Two and three reduction regions are present. Regions I-II and II-III for one day, A-B and B-C for four days, and 1-2 for 14 days were defined by a drop in potential followed by a small plateau, in turn followed by an inflection point. An extensive plateau, regions 2-3 and 3-4 for 14 days, was formed before the second and third inflection points, and after this hydrogen bubbles appeared on the copper surface, and the potential stabilized, an indication that all the corrosion products on the copper had been reduced and that the copper surface was being cleaned. The layer thickness was determined using Faraday's law.[34] Thickness data were calculated by assuming the average density of oxide layers in regions 1-2, A-B, and I-II to be equal to that of amorphous cuprite (6.0 g/cm^3), and in region 2-3, B-C, and II-III equal to that of cuprite (6.0 g/cm^3). Finally region 3-4 was attributed to copper acetate (1.88 g/cm^3). Despite a

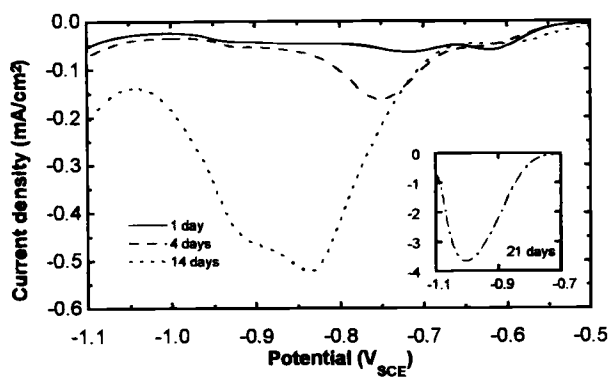

Fig. 4. Reduction scans in a 0.1 M deaerated sodium borate solution for copper exposed to 100 ppm acetic acid vapor. The scans were obtained at a potential sweep rate of 1 mV/s starting at the open-circuit potential.

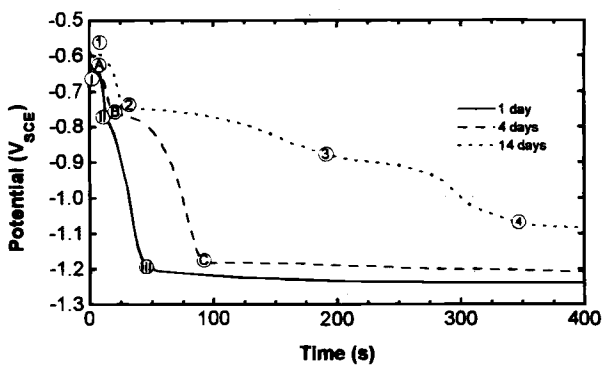

Fig. 6. Cathodic stripping for copper exposed to the action of 10 ppm acetic vapor. A 0.1 M deaerated sodium borate solution was used as supporting electrolyte. Current density, 250 μA/cm².

Table I. Thickness of corrosion-product layer for copper exposed to 10 ppm acetic acid vapor. Exposure time 1, 4, and 11 days.

Time (days)	Region	Compound	Thickness (nm)
1	I-II	Amorphous cuprite	4.0
1	II-III	Cuprite	11.1
4	A-B	Amorphous cuprite	5.9
4	B-C	Cuprite	22.6
11	1-2	Amorphous cuprite	8.7
11	2-3	Cuprite	48.8
11	3-4	Copper acetate	225.4

lack of information about the surface roughness factor of the specimens and assuming the layer to be uniform, the thickness under conditions appertaining to Fig. 6 was approximately as indicated in Table I.

X-ray powder diffraction.—Figure 7 depicts XRD patterns only for specimens exposed to 50, 100, 200, and 300 ppm acetic acid vapor for 21 days. The diagrams corresponding to the specimens exposed to an uncontaminated acetic vapor atmosphere and to 10 ppm of acetic vapor were constructed from direct analysis of the plates. Patterns for the others were recorded from analysis of the powdered solids. In the case of the specimen exposed to 10 ppm acetic vapor, the corrosion layer thickness did not provide an adequate amount of solid corrosion products to record the XRD pattern from the powdered solids. The XRD pattern for the specimens exposed to an uncontaminated atmosphere and to 10 ppm acetic vapor (not included in the figure) showed only the maximum reflections corresponding to metallic copper. Nevertheless the background of the XRD patterns corresponding to the copper specimen exposed to 10 ppm seems to indicate the presence of an amorphous phase. This phase could be uncrystallized cuprite. The crystalline phases observed on the copper specimen exposed to the action of 300 ppm acetic vapor are copper acetate dihydrate $Cu(CH_3COO)_2 \cdot 2H_2O$ [JCPDS 27-145] as the principal component (95%), see Table II, and cuprite Cu_2O [JCPDS 5-667] (5%). This result may explain the copper acetate masking of cathodic reduction peaks described above (Fig. 4 and 5). The XRD patterns for the intermediate contamination specimens, 50 and 100 ppm acetic vapor, show the presence of a third phase, which may be attributed to a copper hydroxide acetate. As can be observed in Fig. 7, this phase (peaks labeled h) starts to form on the 50 ppm acetic contamination specimen, is the principal component on the 100 ppm acetic specimen, and is the minority component on the 200 ppm acetic specimen. In addition to copper hydroxide acetate, all the XRD patterns show cuprite (peaks labeled c) and copper acetate (peaks labeled a). From the intensity values of diffraction maxima, and taking into account only the influence of the copper scattering factor, the relative percentage corresponding to the different crystalline phases formed in the corrosion layer have been calculated. Results are show in Table II. No other factors such as polarization, temperature, particle size, or preferred orientations were considered when determining the phase proportions in the specimens. The presence of basic copper acetate has been observed by some authors on patinas formed on copper exposed to laboratory and outdoor atmospheres.[35] Unfortunately this compound has not been characterized. The XRD pattern of the copper hydroxide acetate observed on the 50 and 100 ppm acetic specimens presents some analogies with the XRD pattern of cobalt hydroxide acetate, $Co_4(OH)(CH_3COO)_7 \cdot 2H_2O$.[36] Assuming that both cobalt and copper hydroxide acetates may be isostructures, the new crystalline phase may be formulated as $Cu_4(OH)(CH_3COO)_7 \cdot 2H_2O$. According to XRD results, the formation of copper hydroxide acetate does not seem to take place from the cuprite layer. Depth-dependent XPS studies indicated a stratified structure from the metal interface to the atmosphere interface: $Cu_2O/CuO/Cu(OH)_2$ or $CuO \cdot xH_2O$ in the first passivating layer.[32,37,38] The presence of hydroxide or hydrated oxide at the initially exposed copper surface provides a building block for the formation of basis copper acetate. The formation of copper hydroxide acetate may be as follows

$$4CuO \cdot xH_2O + 7CH_3COOH \rightarrow Cu_4(OH)(CH_3COO)_7 \cdot 2H_2O + (x + 1)H_2O \quad [6]$$

This copper hydroxide acetate evolves to form copper acetate under the atmospheric conditions of high concentration of acetic acid, by the reaction

$$Cu_4OH(CH_3COO)_7 \cdot 2H_2O + CH_3COOH \rightarrow 4Cu(CH_3COO)_2 \cdot 2H_2O + H_2O \quad [7]$$

the final constituents of the patina being cuprite and copper acetate. Thus, the presence of copper hydroxide acetate among the patina components could mean that the patination process has not yet finished.

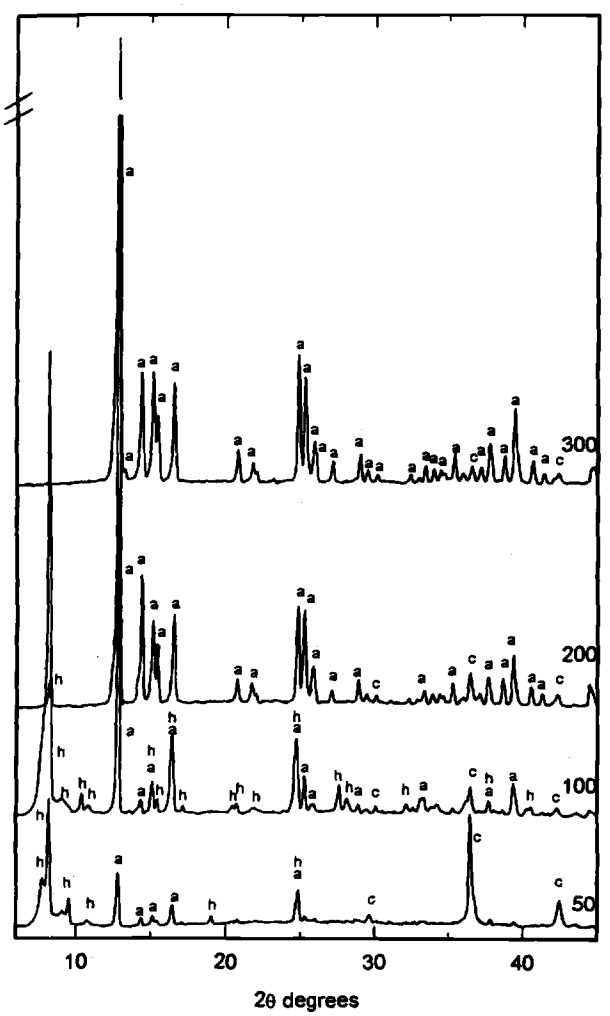

Fig. 7. XRD patterns for copper exposed to 50, 100, 200, and 300 ppm acetic acid vapor for 21 days, c = cuprite, a = copper acetate dihydrate, and h = copper hydroxide acetate.

Table II. Relative percentage of phases formed on copper specimens for 21 days.

Acetic vapor (ppm)	Cuprite (%)	Copper hydroxide acetate (%)	Copper acetate (%)
300	5	—	95
200	6	5	89
100	6	69	25
50	46	45	9

Infrared spectroscopy.—Infrared spectroscopy studies were performed on the powdered samples to confirm the previous results. Figure 8 shows the FTIR spectrum for 10, 50, and 200 ppm acetic acid vapor exposed specimens. Two strong bands at 1570 and 1415 cm^{-1} were observed in the FTIR spectrum of the copper specimen exposed to 10 ppm acetic vapor. These bands correspond, respectively, to asymmetrical (ν_{as}) and symmetrical (ν_s) stretching vibrational modes of a carboxilate group (COO^-). The separation between the two bands of $\Delta = 155$ cm^{-1} corresponds to free acetate groups, and consequently could be attributed to adsorbed acetic acid on the amorphous cuprite phase surface. At 3409 cm^{-1}, a broad and strong band appeared which corresponds to the water molecule stretching vibrational mode. The remainder of the spectrum consisted of weak bands of little practical importance. These results could mean that, in an atmosphere with low acetic concentration, the formation of the first patina layer on copper (cuprite) is due to the reaction of water molecules with copper.

In the FTIR spectrum of the copper specimen exposed to 50 ppm acetic vapor, a shift was observed in the stretching band of water toward a high wavenumber at 3466 cm^{-1}. The ν_{as} band of a COO^- group was split at 1618 and 1570 cm^{-1}, and the ν_s band at 1420 and 1415 cm^{-1}. These results are experimental evidence of acetate groups coordinated with copper, probably through an unidentate link, due to high separation between both asymmetric and symmetric bands (200 cm^{-1}).

The FTIR spectrum of the copper specimen exposed to 100 ppm acetic vapor was similar to that of the 50 ppm acetic acid vapor exposed specimen, with the ν_{as} (COO^-) at 1609 cm^{-1} (very strong) and 1564 cm^{-1} (shoulder) and the ν_s (COO^-) at 1427 cm^{-1} (strong) and 1398 cm^{-1} (shoulder). The separation between the two vibrational modes decreases, which may be interpreted as the buildup of acetate compound with a bridging-type structure between two copper atoms, as occurs in the copper acetate dihydrate structure, $Cu(CH_3COO)_2 \cdot 2H_2O$, which presents a dimeric structure in which two copper atoms are held together by four acetate bridges.[39] This situation is more evident in the FTIR spectrum of the copper specimen exposed to 200 ppm acetic vapor, where the ν_{as} (COO^-) appeared at 1605 and 1560 cm^{-1} and the ν_s (COO^-) shifted to high wavenumbers, at 1448 and 1422 cm^{-1}. The FTIR spectrum of the copper specimen exposed to 300 ppm acetic vapor was similar to the latter, in both cases the water band was observed to have a fine structure with maximums at 2489, 3392, and 3284 cm^{-1}.

Thermogravimetric and thermodifferential analyses.—Figure 9a shows TG and DTA curves corresponding to the copper specimen exposed to 100 ppm acetic vapor. A first weight loss (1.63%) can be observed between 75 and 123°C in the TG curve and is assigned to the dehydration process of copper acetate hydrate. Immediately after, a second weight loss (3.26%) occurs up to 178°C, which may be attributed to dehydroxilation of basic copper acetate, corroborating the above XRD results. These two weight losses correspond with endothermic peaks on the DTA curve centered at 100 and 129°C (see Fig. 9a inset). A third weight loss (21.63%) takes place between 193 and 266°C, attributed to the oxidation of copper acetate to yield tenorite (CuO)

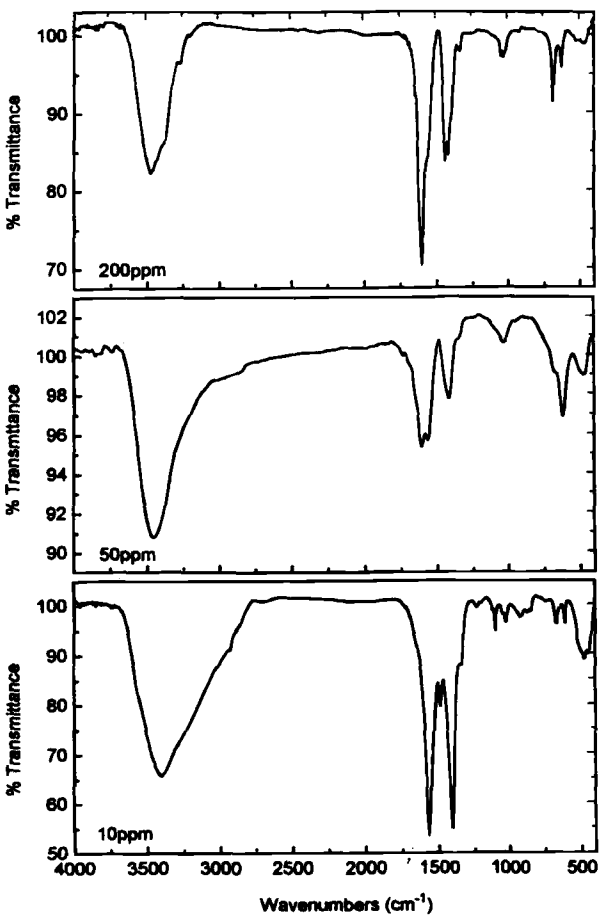

Fig. 8. FTIR spectrum for specimens exposed to 10, 50, and 200 ppm acetic acid vapor for 21 days.

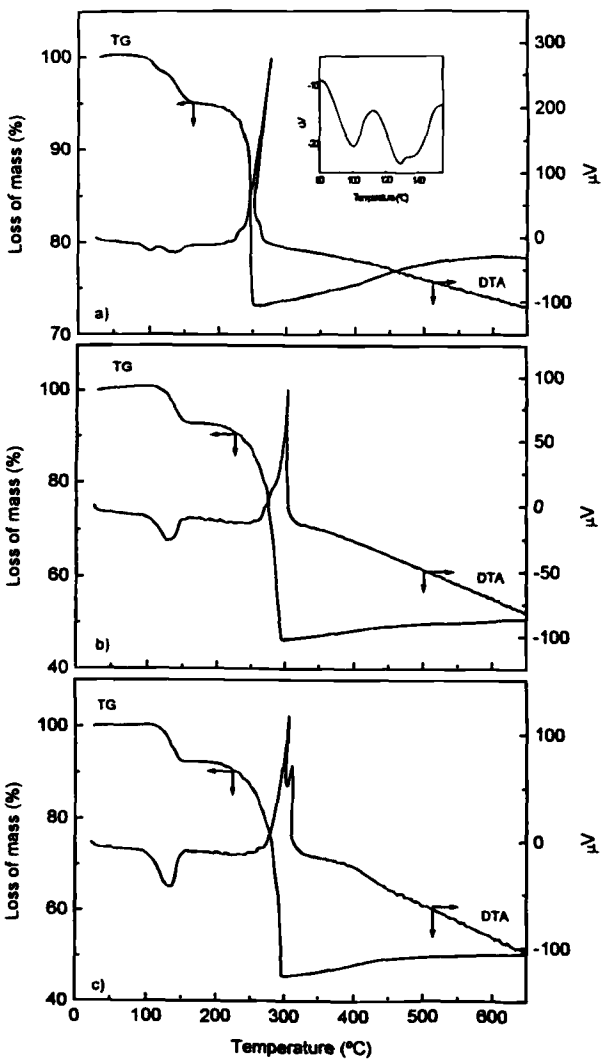

Fig. 9. TG and DTA curves for copper exposed for 21 days to (a) 100, (b) 200, and (c) 300 ppm acetic acid vapor. An inset DTA curve is also included for 100 ppm acetic vapor.

$$Cu(CH_3COO)_2 + 4\ O_2 \rightarrow CuO + 4CO_2 + 3H_2O$$

$$\Delta H = -1614.4\ \text{kJ/mol} \quad [8]$$

Immediately afterward, a weight increase (4.86%) occurs up to 550°C due to the oxidation process of cuprite

$$Cu_2O + \frac{1}{2}O_2 \rightarrow 2CuO \quad \Delta H = -134.7\ \text{kJ/mol} \quad [9]$$

with tenorite being identified by XRD as the final decomposition product. These latter processes are partially overlapped, as is shown by the exothermic process observed in the DTA curve between 220 and 270°C. ΔH at the corresponding temperature has been calculated using the Outokumpu HSC Chemistry 97036-ORC-T program.[40]

Figures 9b and c show TG and DTA curves for the copper specimen exposed to 200 and 300 ppm acetic vapors, respectively. The similar thermal behavior of both samples on curve shape and mass variation corroborate the XRD results. Both samples are formed of a mixture of cuprite and copper acetate, although a very small quantity of copper hydroxide acetate is still present in the copper specimen exposed to 200 ppm acetic vapor. A first weight loss (8.05%) takes place between 85 and 167°C, which is attributed to the dehydration of copper acetate, corresponding with the first endothermic peak on the DTA curve. Afterwards, a weight loss (46.5%) takes place and is attributed to the oxidation of copper acetate, reaction 8, followed by a weight increase (3.5%) attributed to the oxidation of cuprite, reaction 9. In both samples the final product from the decomposition process, identified using the XRD technique, was also tenorite. On the copper specimen exposed to 300 ppm acetic vapor, the two processes, reactions 8 and 9, are more differentiated than in the specimen exposed to 200 ppm acetic vapor, see for instance the peaks at 304 and 310°C of the exothermic process (Fig. 9c).

Scanning electron microscopy.—Figure 10 shows the morphological aspect of a mechanically polished copper specimen obtained by SEM. Figure 10a shows an unexposed mechanically polished copper specimen included as reference, in which the scratched surface can be observed. When copper is exposed to an uncontaminated 100% RH atmosphere for 21 days, the corrosion process starts to occur as can be observed in Fig. 10b. Corrosion starts in the deepest polished line, where little drops of water are more easily retained. Figure 10c shows a SEM micrograph of copper after exposure to 10 ppm acetic vapor for 21 days. It can be observed that the patination process follows the orientation of the polished surface. The nonhomogeneous grain size of this first layer of cuprite is up to 1 μm. This layer is not crystallographically ordered and accordingly is amorphous to the X-ray diffraction.

Figure 11a shows the general appearance of copper exposed to 50 ppm of acetic vapor for 21 days. Two types of droplets can be observed: clear color droplets (labeled 1) and dark color droplets (labeled 2). Both types of droplets are heterogeneous in size (between 0.1 and 0.5 mm diam). Some of these droplets started to run down the vertically suspended copper surface and for this reason present an elongated-circle shape. Figure 11b shows a magnification of a clear droplet in which well-defined cuprite crystals with straight sides and with a size of more than 4 μm can be observed for 21 days. In this figure it is also possible to observe the droplet boundary and the contrast between the lower amorphous layer and the much smaller grain size. Figure 11c shows a magnification of a dark droplet, for 21 days exposure, in which can be seen a dendritic growth of copper hydroxide acetate from the droplet boundary, where the local concentration of acetic acid is higher, toward the interior of the droplet. The formation of copper hydroxide acetate does not seem to occur at the expense of the cuprite layer. The arborescent crystallizations are formed at the expense of acetic vapor which may penetrate to the base copper through porous cuprite paths. According to the reaction products formed under droplets, it may be assumed that clear and dark droplets correspond to water and acetic droplets, respectively.

Figure 12a shows the general appearance of a copper surface exposed to 100 ppm acetic vapor for 21 days exposure. It can be observed that the patina consists of irregular protuberances, such as hollow towers perpendicular to the copper surface. Three different crystal morphologies can be observed which may correspond to copper hydroxide acetate (labeled 1), copper acetate (labeled 2), and cuprite (labeled 3), which also show different developments. Thus, some crystal macles of cuprite of 100 μm size can be observed. Figure 12b presents a SEM micrograph attributed to copper hydroxide acetate for 21 days exposure, with well-formed rectangular prismatic crystals, some of them

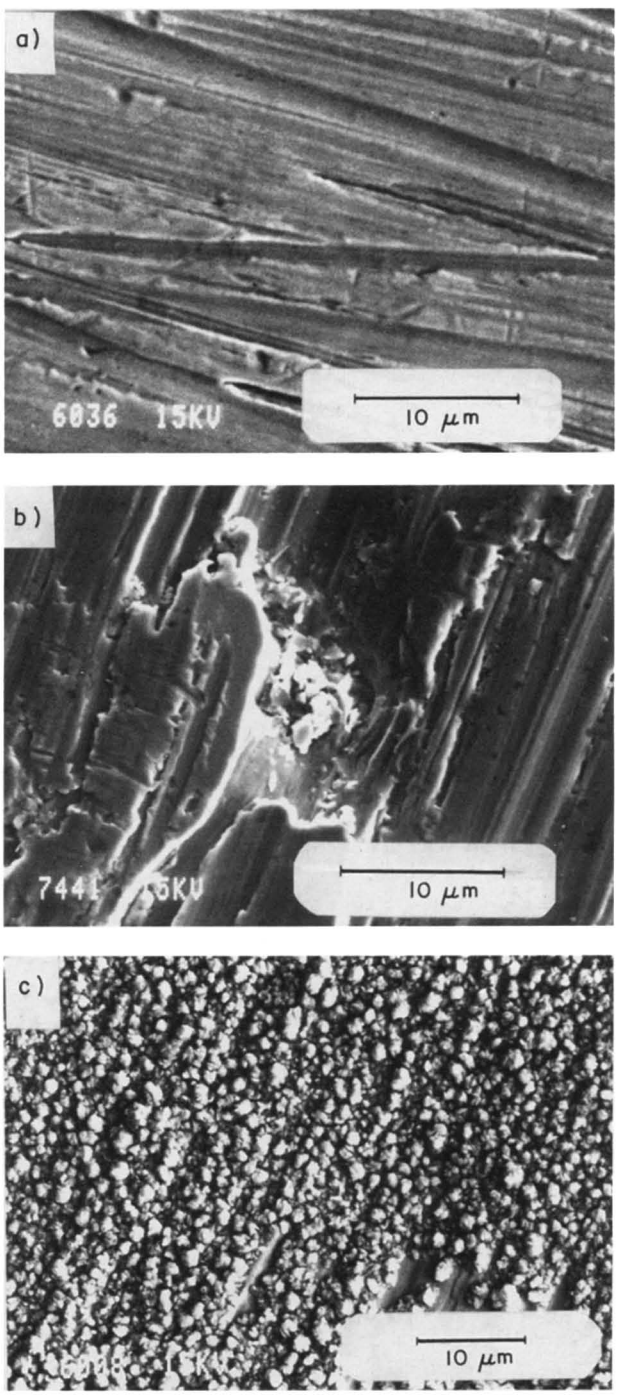

Fig. 10. SEM micrographs for (a) unexposed mechanically polished copper, (b) copper exposed to uncontaminated 100% RH for 21 days, and (c) copper exposed to 10 ppm acetic acid vapor for 21 days.

up to 10 μm in length with well-defined face and sides growing over the lower layer of copper oxide. Another phase with a different crystalline habit can be observed, consisting of small irregular plate-like crystals growing perpendicular to the copper hydroxide acetate phase and attributed to copper acetate. Figure 12c presents a zone with plate-like crystals of copper acetate developed over prisms of copper hydroxide acetate for 21 days exposure.

Figure 13a shows a SEM micrograph of a copper specimen exposed to 200 ppm acetic vapor for 21 days. It is possible to observe plate-like copper acetate crystals over the lower copper oxide phase. It should be pointed out that in this figure the cementation process of small oxide particles to the lower layer is caused by the high concentrations of acetic acid. These results agree well with the mechanisms proposed by Graedel in relation with copper patina formation processes in atmospheres contaminated with organic compounds.[26]

Figure 13b shows a SEM micrograph of a copper specimen exposed to 300 ppm acetic vapor for 21 days. Here the copper acetate layer covers all the copper surface, not only local zones as in the previous sample. In some zones it is possible to observe large cuprite crystals (labeled 1) which arise between the copper acetate crystals, showing an irregular growth pattern due to the high acetic vapor concentration.

Conclusions

Acetic vapor produces a high copper corrosion rate, in the range of 1 to 23 mdd. Under the tested experimental conditions, the effect of 100% RH on the corrosion process is very low and is only observed in small local zones. Low acetic vapor concentrations induce an acceleration of the corro-

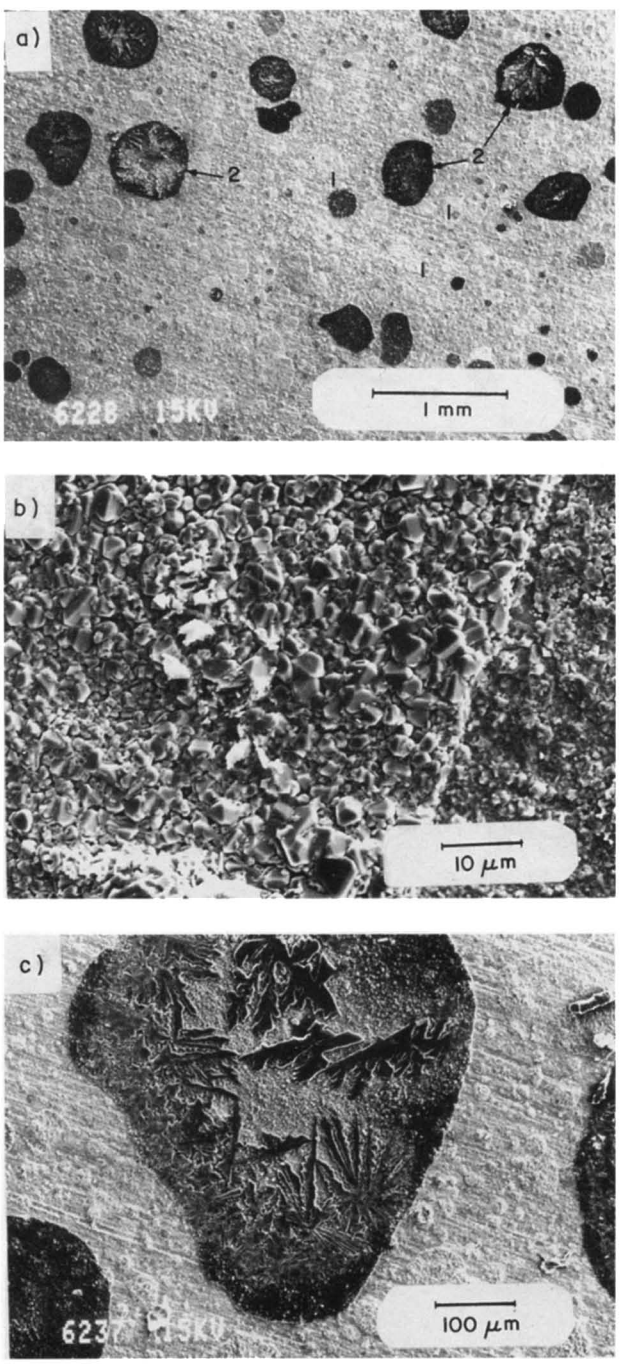

Fig. 11. SEM micrographs for copper exposed to 50 ppm acetic acid vapor for 21 days: (a) general appearance, 1 = water droplet, 2 = acetic droplet, (b) a magnified zone with a water droplet boundary, and (c) a magnified zone with a droplet of acetic acid.

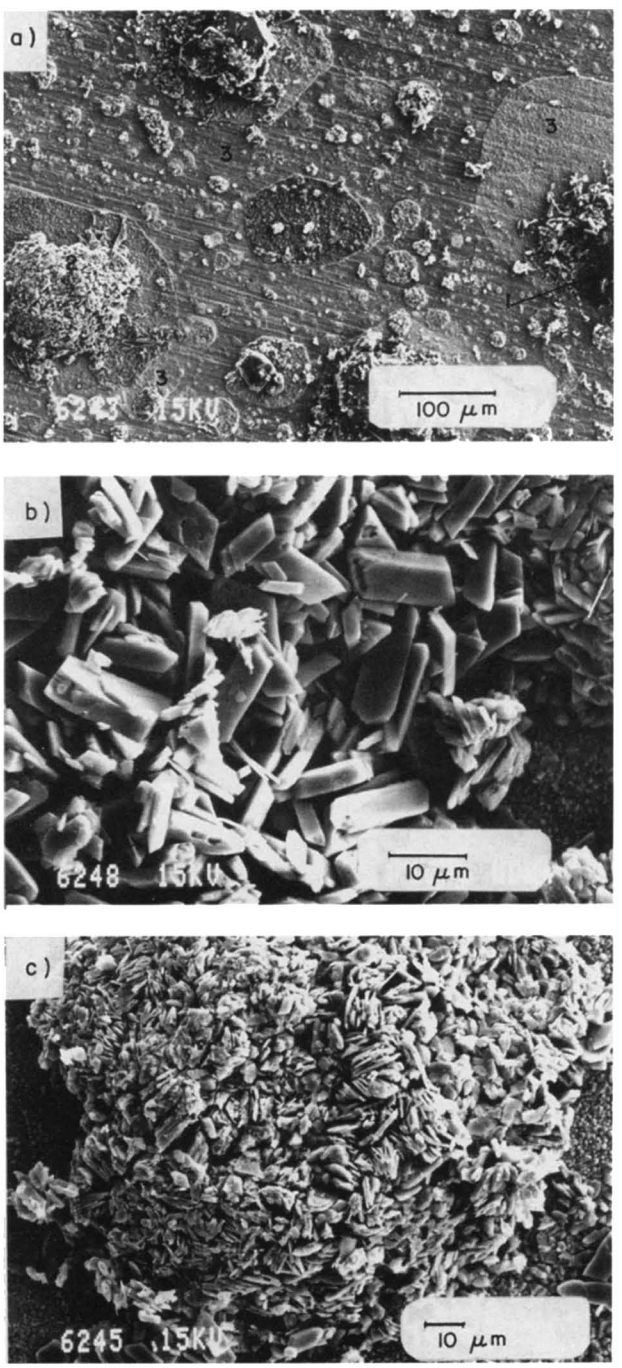

Fig. 12. SEM micrographs for copper exposed to 100 ppm acetic acid vapor for 21 days: (a) general appearance, 1 = copper hydroxide acetate, 2 = copper acetate, 3 = cuprite, (b) copper hydroxide acetate crystals, and (c) copper acetate crystals.

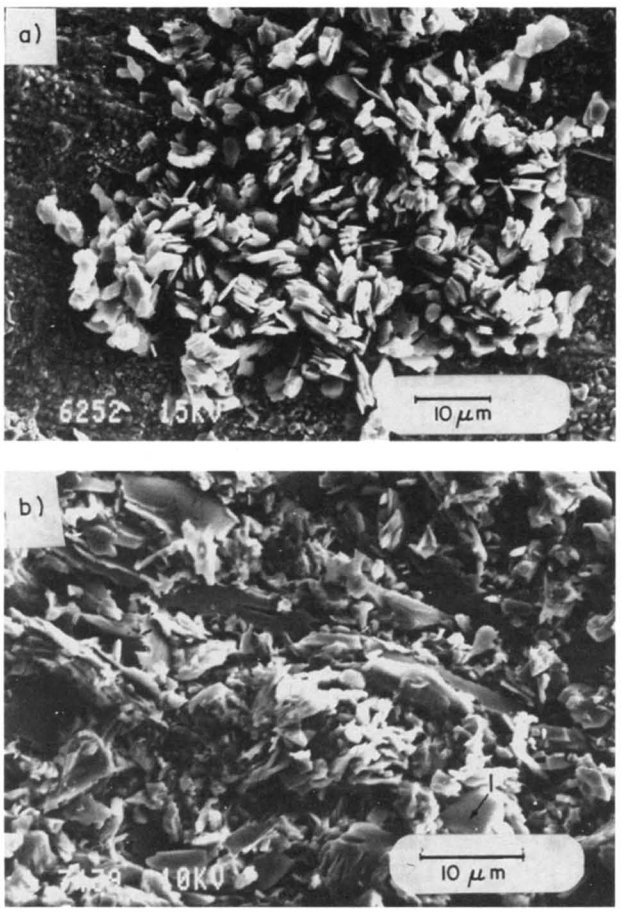

Fig. 13. SEM micrographs for copper exposed to (a) 200 ppm acetic acid vapor and (b) 300 ppm acetic acid vapor, 1 = cuprite, for 21 days.

sion process, and in this case the formation of cuprite takes place in a more or less uniform way over all the copper.

The main components of the patina were cuprite, copper acetate, and copper hydroxide acetate. This last compound has been well characterized in this paper. The experimental results show the influence of acetic vapor on the cementation of patina layers formed on copper. At low acetic concentrations, the molecules enter patination reactions by adsorption from the gas phase to the wetted copper surfaces. The reaction takes place on the adsorbed film of water, and the patina is initially developed in a uniform manner. As the acetic concentration increases, the copper hydroxide acetate and copper acetate start to develop on local zones from droplets of acetic acid adsorbed on the surface. This may indicate that at the highest acetic concentrations the reaction mechanism is different and in this case the molecules enter patination reactions by their incorporation into droplets, followed by the interaction of these droplets with the copper. The presence of basic copper acetate in the patina means that the patination process has not finished and the high acetic vapor concentration continues to modify the patina.

Acknowledgments

The authors express their gratitude to the CICYT of Spain for its financial support for Project no. QUI97-0666-C02-01. E.C. expresses his gratitude to the Spanish Ministry of Education and Culture for the scholarship.

Manuscript submitted April 9, 1998; revised manuscript received August 7, 1998.

Centro Nacional de Investigacions Metalúrgicas assisted in meeting the publication costs of this article.

REFERENCES

1. W. H. J. Vernon, *J. Chem. Soc.*, 1853 (1934).
2. W. C. Keene, J. N. Galloway, and J. D. Holden, Jr., *J. Geophys. Res.*, **88,** 5122 (1983).
3. K. Kawamura and I. R. Kaplan, *Anal. Chem.*, **56,** 1616 (1984).
4. T. E. Graedel, *J. Electrochem. Soc.*, **133,** 2476 (1986); *J. Electrochem. Soc.*, **141,** 922 (1994).
5. Y. Fukuda, T. Fukushima, A. Sulaiman, I. Musalam, L. C. Yap, L. Chotimongkol, S. Judabong, A. Potjanart, O. Keowkangwal, K. Yoshihara, and M. Tosa, *J. Electrochem. Soc.*, **138,** 1238 (1991).
6. W. C. Keene and J. N. Galloway, *Atmos. Environ.*, **18,** 2491 (1984).
7. S. G. Clarke and E. E. Longhurst, *J. Appl. Chem.*, **11,** 435 (1961).
8. T. E. Graedel, C. McCrory-Joy, and J. P. Franey, *J. Electrochem. Soc.*, **133,** 452 (1986).
9. U. R. Evans, *Chem. Ind.*, 706 (1951).
10. G. Schikorr, *Werkst. Korros.*, **12,** 1 (1961).
11. P. C. Arni, G. C. Cochrane, and J. D. Gray, *J. Appl. Chem.*, **15,** 305, 463 (1965).
12. P. D. Donovan, *Protection of Metals From Corrosion in Storage and Transit*, pp. 78-110, Ellis Horwood, Chichester, England (1986).
13. P. D. Donovan and J. Stringer, *Br. Corros. J.*, **6,** 132 (1971).
14. P. D. Donovan and J. Stringer, in *Proceedings of 4th International Congress Metallic Corrosion*, N. E. Hammer, Editor, pp. 537-544, NACE, Houston, TX (1972).
15. D. Cermáková and Y. Vlchkova, in *Proceedings of 3rd International Congress Metallic Corrosion*, Y. M. Kolotyrkin, Editor, pp. 497-508, Moscow (1966).
16. J. M. Bastidas and E. M. Mora, *Can. Metall. Quart.*, **37,** 57 (1998)
17. A. R. Parkinson, *Anti-Corros., Methods. Mater.*, **37,** 11 (1980)
18. D. Knotková-Cermáková and Y. Vlchkova, *Br. Corros. J.*, **6,** 17 (1971).
19. T. Notoya, *J. Mater. Sci. Lett.*, **10,** 389 (1991).
20. H. S. Taylor, *A Treatise of Physical Chemistry*, pp. 359-361, D. Van Nostran, New York (1931).
21. *Handbook of Chemistry and Physics*, 71st ed. D. R. Lide, Editor, pp. 6.54-6.55, CRC Press, Boca Raton, FL (1990).
22. J. M. Bastidas, M. P. Alonso, E. M. Mora, and B. Chico, *Werkst. Korros.*, **46,** 515 (1995).
23. E. M. M. Sutter, C. Fiaud, and D. Lincot, *Electrochim. Acta*, **38,** 1471 (1993).
24. C. Fiaud and N. Guimouz, *Br. Corros. J.*, **24,** 279 (1989).
25. J. Vedel and M. Soubeyrand, *J. Electrochem. Soc.*, **127,** 1730 (1980).
26. T. E. Graedel, *Corros. Sci.*, **27,** 721 (1987).
27. C. Fiaud, M. Safavi, and J. Vedel, *Werkst. Korros.*, **35,** 361 (1984).
28. B. I. Rickett and J. H. Payer, *J. Electrochem. Soc.*, **142,** 3713 (1995).
29. M. Lenglet, K. Kartouni, and D. Delahaye, *J. Appl. Electrochem.*, **21,** 697 (1991).
30. R. L. Deutscher and D. Woods, *J. Appl. Electrochem.*, **16,** 413 (1986).
31. R. E. v. d. Leest, *Werkst. Korros.*, **37,** 629 (1986).
32. Y-Y. Su and M. Marek, *J. Electrochem. Soc.*, **141,** 940 (1994).
33. Y. Feng, W-K. Teo, K-S. Siow, Z. Gao, K-L. Tan, and A-K. Hsieh, *J. Electrochem. Soc.*, **144,** 55 (1997).
34. J. M. Bastidas, A. López-Delgado, F. A. López, and M. P. Alonso, *J. Mater. Sci.*, **32,** 129 (1997).
35. A. López-Delgado, J. M. Bastidas, M. P. Alonso, and F. A. López, *J. Mater. Sci. Lett.*, **16,** 776 (1997).
36. J. L. Doremieux, *Bull. Soc. Chim. Fr.*, 4593 (1967).
37. H.-H. Strehblow and B. Titze, *Electrochim. Acta*, **25,** 839 (1980).
38. E. Otero, J. M. Bastidas, W. López, and J. L. G. Fierro, *Werkst. Korros.*, **45,** 387 (1994).
39. J. Catterick and P. Thornton, *Adv. Inorg. Chem. Radiochem.*, **20,** 291 (1977).
40. A. Roine, Outokumpu Research Oy. Pori, Finland (1992).